

# Homogeneous broadening of the $S$ to $P$ transition in InGaAs/GaAs quantum dots measured by infrared absorption imaging with nanoscale resolution

S. Sauvage,<sup>1,2,\*</sup> A. Driss,<sup>1,2</sup> F. Réveret,<sup>1,2</sup> P. Boucaud,<sup>1,2,†</sup> A. Dazzi,<sup>1,3</sup> R. Prazeres,<sup>1,3</sup> F. Glotin,<sup>1,3</sup> J.-M. Ortéga,<sup>1,3</sup> A. Miard,<sup>4</sup> Y. Halioua,<sup>4</sup> F. Raineri,<sup>4</sup> I. Sagnes,<sup>4</sup> and A. Lemaître<sup>4</sup>

<sup>1</sup>Centre National de la Recherche Scientifique, Orsay F-91405, France

<sup>2</sup>Institut d'Électronique Fondamentale, Université Paris-Sud, UMR8622, Orsay F-91405, France

<sup>3</sup>CLIO-Laboratoire de Chimie Physique, Université Paris-Sud, UMR8000, Orsay F-91405, France

<sup>4</sup>Laboratoire de Photonique et de Nanostructures, Centre National de la Recherche Scientifique, UPR20,

Route de Nozay, Marcoussis F-91460, France

(Received 2 December 2010; published 10 January 2011)

Absorption of single InGaAs self-assembled quantum dots is spatially resolved in resonance with the  $S$  to  $P$  polaron transitions around  $\lambda = 25 \mu\text{m}$  wavelength. We show that the spatial resolution down to 50 nm ( $\lambda/500$ ) combined with the analysis of the absorption nanoscopy images provides a measurement of the homogeneous broadening at room temperature. The  $2.5 \pm 1$  meV measured  $S$ - $P$  homogeneous broadening supports the calculated value accounting for acoustic phonon-induced decoherence.

DOI: [10.1103/PhysRevB.83.035302](https://doi.org/10.1103/PhysRevB.83.035302)

PACS number(s): 78.67.Hc, 07.79.Lh, 73.21.La, 78.30.Fs

## I. INTRODUCTION

The spatial and spectral resolution of optical absorptions at the nanometer scale is a fundamental step for the exploration and control of nanomaterial properties.<sup>1</sup> While nanoscopy allows us to perform spatial measurements at the single nanostructure level, absorption spectral resolution and linewidth measurements represent direct signatures of the coupling to the environment.<sup>2</sup> On single semiconductor nanostructures with large absorption cross sections or metallic nanostructures, various all-optical nanoscopies have been successfully carried out such as apertureless near-field optical measurements,<sup>3</sup> photothermal imaging,<sup>4,5</sup> and nonlinear susceptibility-sensitive heterodyne detection in the visible spectral range.<sup>6</sup>

Absorption nanospectroscopy is particularly challenging for long wavelengths  $\lambda$  because it requires us to achieve measurements well below the diffraction limit ( $\sim\lambda/2$ ). Measuring absorption homogeneous linewidths down to single semiconductor quantum dots (QDs) in the far-infrared spectral range is challenging. The QDs are nearly transparent and are expected to exhibit very small transmission variations ( $\sim 10^{-9}$ ) in a diffraction-limited setup.<sup>7</sup> If single QD addressing is reached, absorption spectral broadening resolution generally requires tunability in the spectral domain or a pulsed source in the time domain with a pulse duration smaller than the decoherence time.

The transition between the  $S$  ground state to the  $P$  first excited state is a model system in quantum mechanics and a model transition to investigate the physics of both self-assembled<sup>8</sup> and colloidal QDs.<sup>9</sup> In the popular InGaAs-GaAs self-assembled system, the  $S$ - $P$  transition absorbs around  $\lambda \sim 25 \mu\text{m}$  wavelength in the far-infrared spectral range. Far-infrared properties of semiconductor QDs have been thoroughly investigated for more than 15 years.<sup>10</sup> So far, QD ensemble distributions have been the preferred studied system, motivated in particular by the QD potential for infrared thermal photodetection.<sup>11</sup> These investigations include absorption,<sup>8</sup> photocurrent,<sup>11</sup> second-harmonic generation,<sup>12</sup> frequency tripling,<sup>13</sup> magnetospectroscopy demonstrating a strong electron-optical phonon coupling regime,<sup>14</sup> and the

formation of polaron states,<sup>15</sup> relaxation dynamics above<sup>16,17</sup> and below the optical phonon energy,<sup>18</sup> optical Rabi oscillation,<sup>19</sup> and dephasing at low temperature.<sup>20</sup> The homogeneous linewidth of the  $S$ - $P$  transition has been previously investigated by photo echoes at low temperature, showing a relaxation-limited linewidth.<sup>20</sup> Because of the need for large absorption amplitudes, the photon echo approach has been limited to QD ensembles and temperatures below 150 K. At the single QD level, the ultrasmall electronic absorption at room temperature has been measured by detecting locally the semiconductor matrix-induced deformation.<sup>7</sup> This has been achieved previously only in resonance with a weak  $S$ - $D$  transition around  $10 \mu\text{m}$  wavelength in the transparent region of the GaAs substrate.

We report on the nanoscopy of the far-infrared absorption of single InGaAs-GaAs QDs in resonance with the model  $S$ - $P$  polaron transition. We show that even without using pump-source spectral tunability, we can extract locally the homogeneous broadening of the  $S$ - $P$  transition through absorption imaging with nanoscale resolution. The analysis of the absorption image represents a transposition of a spectral hole-burning experiment into the spatial domain. The measured homogeneous broadening is compared favorably to the nonperturbative calculation of the  $S$ - $P$  transition dephasing recently reported in the literature, accounting for acoustical phonon-induced decoherence.<sup>21,22</sup>

## II. SAMPLES AND EXPERIMENTS

Measuring the ultrasmall  $S$ - $P$  absorption of single InGaAs-GaAs QDs around  $\lambda \sim 25 \mu\text{m}$  wavelength requires us to overcome the nontransparency of the GaAs substrate.<sup>23</sup> Technological steps are thus achieved to bury a single QD plane into a thin 300-nm-thick GaAs membrane. This membrane is glued onto a transparent silicon substrate with a far-infrared transparent glue made of benzocyclobutene (BCB), as schematically depicted in Fig. 1(a).

Contrarily to a bulk GaAs-based structure, all 280- $\mu\text{m}$ -thick silicon, BCB, and GaAs thin membranes are nearly

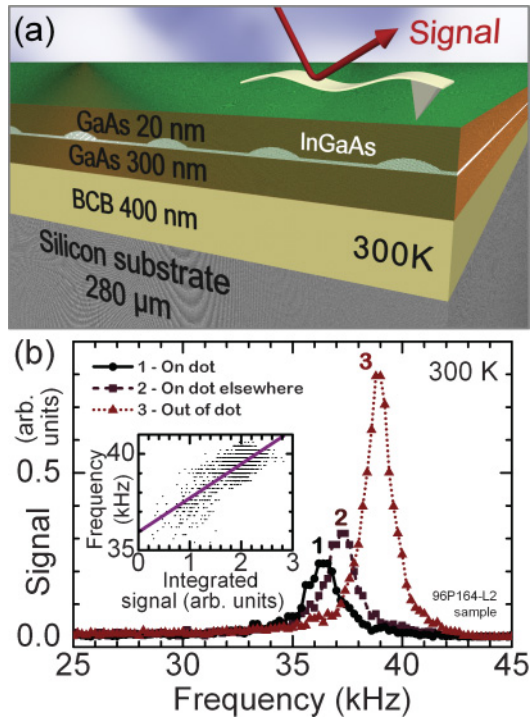


FIG. 1. (Color online) (a) Schematic sample structure and experimental AFM configuration for the measurement of the buried QD absorption. The AFM tip and thicknesses are not to scale. (b) Mechanical oscillation amplitude (i.e., absorption signal) of the cantilever as a function of frequency for three different points on the surface. These points are labeled 1, 2, and 3. In the inset, the dots report the systematic experimental shift of the cantilever oscillation frequency with respect to the absorption signal. The violet solid line is a best linear fit to guide the eye.

transparent around 50 meV with absorptance (respectively, absorption) around 0.05% ( $14.7 \text{ cm}^{-1}$ ) for GaAs,<sup>23</sup> 1.2% ( $0.45 \text{ cm}^{-1}$ ) for Si,<sup>23</sup> and 0.8% ( $200 \text{ cm}^{-1}$ ) for BCB, measured by Fourier transform spectroscopy on a 40- $\mu\text{m}$ -thick BCB reference layer. Note that the residual absorptions of GaAs, BCB, and Si are expected to be spatially uniform and therefore are not expected to contribute to the nanoscopy image contrast formation.

QD sheet density is  $n_0 = 4 \times 10^{10} \text{ cm}^{-2}$ . Calculation shows that a doping sheet density of  $4 \times 10^{11} \text{ cm}^{-2}$  ensures approximately one electron in average in the  $S$  ground state at room temperature. The absorption measurement is based on the free electron laser CLIO at Orsay and is measured at room temperature with the tip of an atomic force microscope (AFM) by sensing the local surface deformation generated by the buried QD absorption in a step-scan mode.<sup>7,24</sup> Note that a similar setup has been considered recently in top-down illumination configuration for the measurement of polystyrene bead absorption.<sup>25</sup> AFM-based scanning capacitance spectroscopy has also been developed recently on single QDs.<sup>26</sup>

### III. ABSORPTION NANOSCOPY

Figure 1(b) presents the mechanical oscillation spectrum of the cantilever on different typical points of the sample surface. These points are labeled 1, 2, and 3. The corresponding

transient oscillation (not shown) follows the 9- $\mu\text{s}$ -long macropulse containing 300 pulses of  $\sim 3$  ps duration at 49.5 meV energy. The macropulses are repeated at 25 Hz. Frequency for the transient cantilever oscillation is around 40 kHz in contact mode. The roughly constant 1.6-kHz spectral width of the spectra corresponds to an oscillation damped within a 1-ms time scale. The striking feature is the strong variation by more than a factor of 3 of the oscillation amplitude for different locations on the surface. This oscillation amplitude variation is the signature of the QD absorption buried 20 nm beneath the surface, as shown later.

The oscillation frequency also varies on these three points and more generally on the sample surface from 36 to 41 kHz. The frequency varies consistently with oscillation amplitude, with a relation that is roughly linear, as shown in the inset of Fig. 1(b). Therefore frequency is also a relevant quantity very sensitive to ultrasmall absorption of the buried QDs. The frequency variation in contact mode is attributed to the modification of the lateral forces at the end of the tip while shifting during oscillations, that is, the modification of the limit conditions of the cantilever oscillation, which depends on its oscillation amplitude.

The absorption-triggered oscillations are better analyzed as a function of position, as reported in Fig. 2(a). For each pixel, the oscillation spectrum is first integrated over the whole spectral resonance from 33 to 47 kHz. The resulting signal is directly related to the absorption<sup>27</sup> and is referred to as absorption signal or simply as the signal in what follows. The absorption signal image exhibits a strong contrast going from 0.5 to 2.5. One clearly distinguishes few low-signal areas, defined as spots, superimposed on a rather uniform high-signal background. The spots on the image are attributed to the absorption from the QDs buried 20 nm beneath the surface. The observation of spots in the two-dimensional image means that the QD absorption signal is consistently scanned from one line to the next after several minutes' duration.

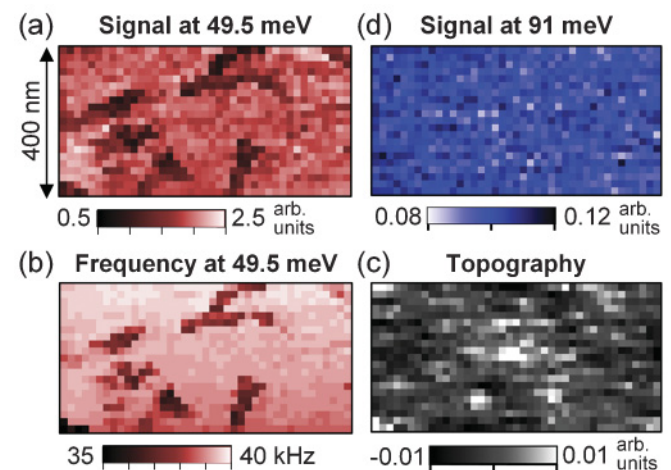


FIG. 2. (Color online) (a) Absorption signal nanoscopy at 49.5 meV (25  $\mu\text{m}$  wavelength). (b) Cantilever oscillation frequency on the same scanned surface. (c) Topography measured during the step-scan absorption signal acquisition. (d) Absorption signal nanoscopy at 91 meV (13.6  $\mu\text{m}$  wavelength) in the transparent spectral region of the QDs.

The signal variation is opposed to the one observed in Ref. 7, which occurs in the transparent region of GaAs. This opposed dependence with absorption has been also observed for absorbing  $\text{SiO}_2$  microdisks around  $20 \mu\text{m}$  wavelength.<sup>27</sup> It is attributed to different phase-delayed thermal interfering contributions to the tip and cantilever excitation originating from various buried absorbing thin layers.<sup>28</sup> A detailed discussion and theoretical description of this thermal phase variation are beyond the scope of this paper. However, this feature is particularly promising since it demonstrates that phase contrasts can be achieved with the AFM absorption imaging in contact mode. Like for all-optical scanning near-field microscopy (SNOM), phase sensitivity is of high interest for imaging.<sup>29</sup> For example, optical contrast reversals are similarly observed on apertureless SNOM<sup>30</sup> because of complex dielectric variation from different SiC polytypes<sup>31</sup> or from germanium self-assembled QDs grown on silicon substrates.<sup>32</sup>

The observation of absorption signal spots is confirmed and better evidenced in the frequency image of Fig. 2(b). Like the signal image, the frequency image also exhibits strong line-to-line correlations, forming spots of two to four pixel sizes. The spatial resolution is therefore of the order of  $\sim 50 \text{ nm}$ , that is,  $\lambda/500$ , well below the diffraction limit.

The surface topography can be measured during the image formation. The topography average deflection signal is reported in Fig. 2(c). The topography measured during the scan is essentially uniform, though some small topography bumps can be observed, in particular, in the middle of the image. The middle of the image does not correspond to any absorption signal variation. Therefore the absorption signal image or frequency image is not generated by topographic features. Topography is also measured just prior to measurement in continuous rapid-scan mode (not shown) and does not reveal any contrast that would be correlated with the absorption image either.

In Fig. 3, the absorption signal, frequency, and topography are complementarily analyzed by looking along scan lines where topography is very flat. Point 3 is free from absorption signal variation. The signal reveals a group of absorbing QDs at point 2 and an absorbing single QD at point 1. Note that the absorption signal is uniform when optically pumped far from the QD resonance. This is illustrated in the nanoscopy of Fig. 2(d) and in Figs. 3(a)–3(b) along a scan line at 91 meV. This 91-meV energy is above the  $S$ - $P$  absorption energy around 50 meV and below the  $S$ - $D$  absorption energy around 105–120 meV.<sup>8</sup> The full line in Fig. 3(c) shows that the topography is regular along the scan line, in contrast to other locations of the samples, reported as a light dotted line, as a result of the technological steps.

#### IV. HOMOGENEOUS BROADENING MEASUREMENT

We show now that the number of observed QDs results from the homogeneous versus inhomogeneous broadenings of the absorbing  $S$ - $P$  transitions. If there were no inhomogeneous broadening, all the QDs would be absorbing equally the pumping laser (assuming equal thermal population for simplicity). In this case, considering that the signal spatial extent ( $\sim 50 \text{ nm}$ ) is close to the average distance between the QDs (50 nm), one

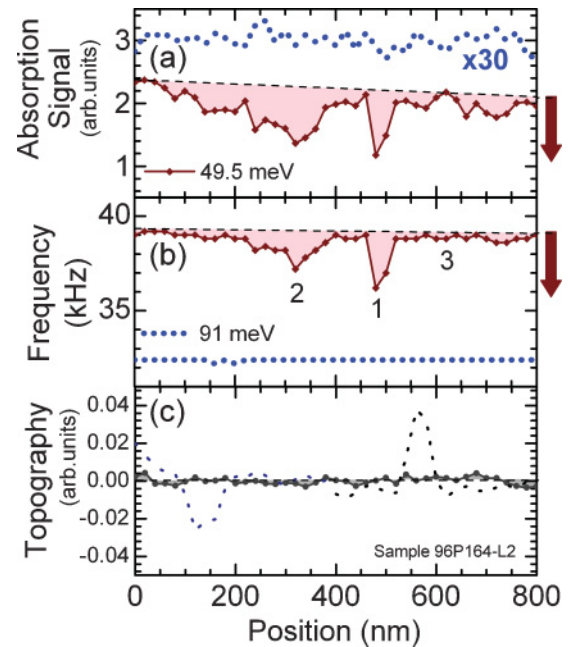


FIG. 3. (Color online) (a) Absorption signal along a 800-nm-long scan line at 49.5 meV (red solid line) and along another scan line at 91 meV (blue dotted line). (b) Cantilever oscillation frequency along the previous scan lines at 49.5 and 91 meV energies. Points 1, 2, and 3 are referring to Fig. 1(b). At 91 meV, the average frequency is different than at 49.5 meV because we have used another cantilever. Frequency discretization sampling is 0.2 kHz. The thick arrows on the right indicate the data variation in the presence of absorption. (c) Topography measured simultaneously by the AFM during the line scan at 49.5 meV. For comparison purposes, the light dotted line reports the topography measured elsewhere above a topographic dip and a topographic bump.

would expect the image to be fully covered with absorption signed pixels corresponding to the 128 QDs statistically buried beneath the surface. This is obviously not the case, and only a limited fraction of the QDs is observed on the absorption signal images. A deviation from this ideal situation is attributed to the  $\hbar\Gamma$  inhomogeneous broadening of the absorption, which translates into absorption energy variation from dot to dot, preventing strong resonances with the laser. Let us define an absorption signature when the oscillation frequency is significantly below 39 kHz. This definition corresponds to pixels for which the signal variation is at least half of the image maximum signal variation. Since only  $\eta = 15\%$  of the surface is covered with an absorption signature, one can estimate the order of magnitude of the QD absorption  $\hbar\gamma$  homogeneous broadening around  $\hbar\gamma = \eta\hbar\Gamma$ . Ensemble absorption spectroscopy gives  $\hbar\Gamma = 13 \text{ meV}$  at room temperature for a reference 80 QD plane sample with a  $1.2 \times 10^{11} \text{ cm}^{-2}$  doping level close to the doping level of the studied sample. One deduces roughly an estimate of the homogeneous broadening at room temperature  $\hbar\gamma \sim 2 \text{ meV}$  in this case. Note that the spectral linewidth  $\Delta\lambda/\lambda$  of the laser pulses is around 0.4% of the  $25\text{-}\mu\text{m}$  wavelength, that is,  $\sim 0.1 \text{ meV}$ , much smaller than the deduced homogeneous broadening  $\hbar\gamma$ . Therefore the 2-meV homogeneous broadening estimate is not limited by the laser linewidth.

This analysis can be seen as a transposition of a spectral hole-burning experiment in the spatial domain. In a typical spectral hole-burning experiment, one saturates the absorption of an inhomogeneous QD distribution with a monochromatic laser (see, e.g., Ref. 9). Absorption bleaching only occurs for those QDs that are in spectral resonance with the laser, within the homogeneous broadening. One then observes a spectral hole in the absorption spectra corresponding to this absorption bleaching. The width of this spectral hole reveals the homogeneous broadening. In our analysis, absorption only occurs for those QDs that are in spectral proximity with the laser line, within the homogeneous broadening. One then observes absorption pixels on the absorption signal image corresponding to absorbing QDs. The number of observed QDs in the image reveals the homogeneous broadening of the QD absorption.

A more realistic estimate of  $\hbar\gamma$  is obtained by accounting for the random character of the QD distribution in the absorption image formation and the thermal population variation from QD to QD, as shown in Fig. 4. The corresponding numerical simulations are based on Lorentzian-shaped absorptions and a Fermi–Dirac thermal distribution for the polarons. We assume a constant oscillator strength for the  $S$ - $P$  transition. A series of random distributions of QD positions and electronic structures are considered based on the typical calculated electronic structure described in Ref. 8. For each distribution,

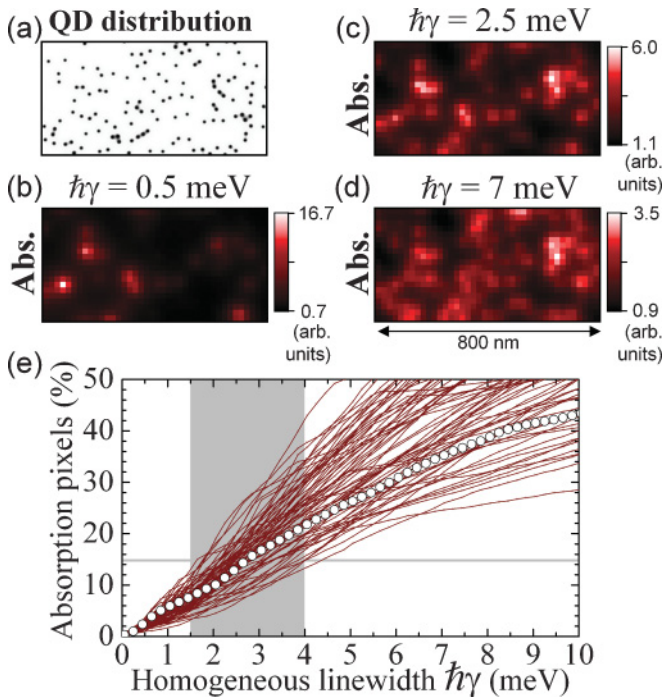


FIG. 4. (Color online) (a) Random spatial distribution of QDs in the plane for the simulation of one typical absorption nanoscopy image. (b–d) Calculated absorption images for a homogeneous Lorentzian FWHM  $\hbar\gamma$  of 0.5, 2.5, and 7 meV. (e) Plot of the relative fraction in percentage (%) of absorption pixels predicted in a series of  $800 \times 400$  nm<sup>2</sup> images as a function of the homogeneous Lorentzian FWHM of the  $S$ - $P$  intersublevel transition at 50 meV. The spatial and spectral QD distribution varies randomly from curve to curve. To guide the eye, one of the curves is singled out with open circles.

such as the one in Fig. 4(a), one calculates absorption images such as Figs. 4(b)–4(d) and reports the number of absorption signed pixels as a function of the  $\hbar\gamma$  homogeneous broadening, as shown in Fig. 4(e);  $\hbar\gamma$  is defined as the full width at half maximum (FWHM) of the Lorentzian shape. From a  $\eta = 15\%$  coverage of the image with absorption pixels, one deduces a more realistic statistical  $\hbar\gamma = 2.5 \pm 1$  meV homogeneous broadening, close to the previous 2-meV estimate.

Let us define the image contrast as the maximum over the minimum absorption amplitudes. The calculated image contrast equals 5.5 and is very close to the measured contrast, which is 5.0. This contrast is significantly larger than the contrast of 2 calculated and observed on the  $S$ - $D$  transition at 120 meV around  $10 \mu\text{m}$  wavelength.<sup>7</sup> As the simulation shows, there are two main reasons explaining this contrast increase. The first reason is the relative increase of the  $S$ - $P$  absorption amplitude as compared to the background absorption. The background absorption originates from the residual and enhanced free carrier absorption at longer 25- $\mu\text{m}$  wavelength. The second reason is the smaller 2.5-meV homogeneous broadening of the  $S$ - $P$  transition as compared to the 10-meV width of the  $S$ - $D$  transition. The smaller linewidth leads directly to a smaller number of quantum dots spectrally resonant with the laser line. Hence one expects a relative smaller background absorption in the image where each quantum dot contribution is more favorably singled out, as seen in Fig. 4. Note that this contrast increase from 2 to 5.5 is not only predicted but also quantitatively observed experimentally and in agreement with the image simulations.

## V. DISCUSSION

We now discuss several decoherence sources leading to the measured 2.5-meV effective homogeneous broadening of the  $S$ - $P$  transition at room temperature. The experimental  $\hbar\gamma$  broadening can be compared to the theoretical line shape recently calculated by Grange *et al.*<sup>21,22</sup> For intersublevel polaron transitions, Grange *et al.* accounts for up to two acoustic phonon decoherence processes in a nonperturbative treatment. In this case, the calculated homogeneous line shape at 300 K for the lower energy  $S$ - $P$  transition is composed of a zero-phonon line (ZPL) superimposed on acoustic phonon sidebands. The ZPL originates both from population decay and from the off-diagonal part of the electron, acoustical phonon interaction leading to real and virtual transitions from the  $P$ -state toward the upper energy  $P$ -state with one or two acoustic phonons. At room temperature, the ZPL exhibits a FWHM of 0.7 meV.<sup>22</sup> On the other hand, the phonon sidebands are nearly as intense and originate from the diagonal part of the electron–acoustical phonon interaction. The phonon sideband spectral FWHM is as large as  $\sim 4$  meV. These theoretical homogeneous linewidth contributions depend on the  $P$  state average splitting. A 5-meV splitting is considered in Fig. 2 of Ref. 22, close to the average 7-meV measured one in the ensemble reference sample.

Our measured 2.5-meV effective homogeneous broadening assuming a Lorentzian line shape is therefore consistent with the typical width of the  $S$ - $P$  transition calculated at room temperature to be between 0.7 and 4 meV. Note that this conclusion

is in contrast with intersubband transitions in GaAs quantum wells.<sup>33</sup> In the latter case, the larger homogeneous broadenings are found to be limited by interface roughness scattering up to room temperature. Another source of broadening is the electron-electron interaction between the electron that thermally populates the  $S$  ground state at room temperature with the other electrons thermally occupy the excited states and the remaining delocalized free electrons in the barriers estimated theoretically around 60% of the doping density. This Coulomb interaction contribution could be reduced by considering low doping density samples, at the expense of a much lower image contrast.<sup>7</sup>

We now compare the data for the  $S$ - $P$  and  $S$ - $D$  transitions. The 2.5-meV effective broadening for the  $S$ - $P$  transition is 4 times smaller than the 10-meV linewidth measured on the  $S$ - $D$  transition.<sup>7</sup> We attribute this narrower broadening to a consequence of the better confinement of  $P$  levels as compared to  $D$  levels. The  $S$ - $D$  transition energy is indeed predicted and observed around 120 meV, while the barrier height from the  $S$  state to the wetting layer continuum is around 150 meV, much closer to the  $D$  levels than to the  $P$  levels. Note that the 2.5-meV effective broadening remains compatible with the slight increase of the ensemble absorption width of the  $S$ - $P$  transition from low temperature to room temperature.<sup>34</sup> At low temperature, the  $\hbar\gamma$  homogeneous linewidth is 2 orders of magnitude smaller, around 16  $\mu\text{eV}$ , as measured by time-domain photon echo on ensemble QDs.<sup>20</sup> In the

latter case, the linewidth is essentially limited by polaron relaxation.

## VI. CONCLUSION

In conclusion, the  $S$ - $P$  polaron absorption of single QDs is spatially resolved at  $\lambda = 25 \mu\text{m}$  with a 50-nm spatial resolution ( $\lambda/500$ ). Using statistical arguments, homogeneous broadening is extracted from absorption nanoscopy and is shown to be consistent with calculation, accounting for acoustic phonon-induced decoherence. AFM-based absorption nanoscopy appears very promising for future demonstrations of high-contrast imaging in the far infrared on various systems of nanometric sizes and local ultrasmall absorption linewidth measurements. Even without pump-source spectral tunability, one can extract local homogeneous broadenings through absorption imaging with nanoscale resolution.

## ACKNOWLEDGMENTS

The authors acknowledge stimulating discussions with T. Grange and R. Ferreira on the polaron decoherence theory. This work has been supported by the Région Ile-de-France in the framework of C’Nano IdF and by Triangle de la Physique; it has also been supported by the French National Agency (ANR) in the framework of its program in Nanosciences and Nanotechnologies (SONORE Project No. ANR-08-NANO-016).

\*sebastien.sauvage@ief.u-psud.fr

†philippe.boucaud@ief.u-psud.fr

<sup>1</sup>S. W. Hell, *Science* **316**, 1153 (2007).

<sup>2</sup>K. Karrai and R. J. Warburton, *Superlattices Microstruct.* **33**, 311 (2003).

<sup>3</sup>B. Knoll and F. Keilmann, *Nature (London)* **399**, 134 (1999).

<sup>4</sup>D. Boyer, P. Tamarat, A. Maali, B. Lounis, and M. Orrit, *Science* **297**, 1160 (2002).

<sup>5</sup>S. Berciaud, L. Cognet, and B. Lounis, *Nano Lett.* **5**, 2160 (2005).

<sup>6</sup>J. R. Guest, T. H. Stievater, G. Chen, E. A. Tabak, B. G. Orr, D. G. Steel, D. Gammon, and D. S. Katzer, *Science* **293**, 2224 (2001).

<sup>7</sup>J. Houel, S. Sauvage, P. Boucaud, A. Dazzi, R. Prazeres, F. Glotin, J.-M. Ortéga, A. Miard, and A. Lemaître, *Phys. Rev. Lett.* **99**, 217404 (2007).

<sup>8</sup>P. Boucaud, S. Sauvage, and J. Houel, *C. R. Phys.* **9**, 840 (2008).

<sup>9</sup>M. Shim and P. Guyot-Sionnest, *Phys. Rev. B* **64**, 245342 (2001).

<sup>10</sup>H. Drexler, D. Leonard, W. Hansen, J. P. Kotthaus, and P. M. Petroff, *Phys. Rev. Lett.* **73**, 2252 (1994).

<sup>11</sup>K. W. Berryman, S. A. Lyon, and M. Segev, *Appl. Phys. Lett.* **70**, 1861 (1997).

<sup>12</sup>S. Sauvage, P. Boucaud, T. Brunhes, F. Glotin, R. Prazeres, J.-M. Ortéga, and J.-M. Gérard, *Phys. Rev. B* **63**, 113312 (2001).

<sup>13</sup>S. Sauvage, P. Boucaud, F. Glotin, R. Prazeres, J.-M. Ortéga, A. Lemaître, J.-M. Gérard, and V. Thierry-Mieg, *Phys. Rev. B* **59**, 8930 (1999).

<sup>14</sup>P. A. Knipp, T. L. Reinecke, A. Lorke, M. Fricke, and P. M. Petroff, *Phys. Rev. B* **56**, 1516 (1997).

<sup>15</sup>S. Hameau, Y. Guldner, O. Verzellen, R. Ferreira, G. Bastard, J. Zeman, A. Lemaître, and J. M. Gérard, *Phys. Rev. Lett.* **83**, 4152 (1999).

<sup>16</sup>S. Sauvage, P. Boucaud, R. P. S. M. Lobo, F. Bras, G. Fishman, R. Prazeres, F. Glotin, J.-M. Ortéga, and J.-M. Gérard, *Phys. Rev. Lett.* **88**, 177402 (2002).

<sup>17</sup>E. A. Zibik *et al.*, *Phys. Rev. B* **70**, 161305 (2004).

<sup>18</sup>E. A. Zibik *et al.*, *Nat. Mater.* **8**, 803 (2009).

<sup>19</sup>F. Bras, S. Sauvage, G. Fishman, P. Boucaud, J.-M. Ortéga, and J.-M. Gérard, *Europhys. Lett.* **70**, 390 (2005).

<sup>20</sup>E. A. Zibik *et al.*, *Phys. Rev. B* **77**, 041307 (2008).

<sup>21</sup>T. Grange, *Phys. Rev. B* **80**, 245310 (2009).

<sup>22</sup>T. Grange, R. Ferreira, and G. Bastard, *J. Phys. Conf. Ser.* **193**, 012129 (2009).

<sup>23</sup>J. I. Pankove, *Optical Processes in Semiconductors* (Dover, Mineola, New York, 1975).

<sup>24</sup>A. Dazzi, R. Prazeres, F. Glotin, and J.-M. Ortéga, *Opt. Lett.* **30**, 2388 (2005).

<sup>25</sup>G. A. Hill, J. H. Rice, S. R. Meech, D. Q. M. Craig, P. Kuo, K. Vodopyanov, and M. Reading, *Opt. Lett.* **34**, 431 (2009).

<sup>26</sup>J. Smoliner, W. Brezna, P. Klang, A. M. Andrews, and G. Strasser, *Appl. Phys. Lett.* **92**, 092112 (2008).

<sup>27</sup>J. Houel, E. Homeyer, S. Sauvage, P. Boucaud, A. Dazzi, R. Prazeres, and J.-M. Ortéga, *Opt. Express* **17**, 10887 (2009).

<sup>28</sup>A. Rosencwaig and A. Gersho, *J. Appl. Phys.* **47**, 64 (1976).

- <sup>29</sup>R. Hillenbrand and F. Keilmann, *Phys. Rev. Lett.* **85**, 3029 (2000).
- <sup>30</sup>S. C. Kehr, M. Cebula, O. Mieth, T. Härtling, J. Seidel, S. Grafström, L. M. Eng, S. Winnerl, D. Stehr, and M. Helm, *Phys. Rev. Lett.* **100**, 256403 (2008).
- <sup>31</sup>N. Ocelic, A. Huber, and R. Hillenbrand, *Appl. Phys. Lett.* **89**, 101124 (2006).
- <sup>32</sup>Y. Ogawa, F. Minami, Y. Abate, and S. R. Leone, *Appl. Phys. Lett.* **96**, 063107 (2010).
- <sup>33</sup>T. Unuma, T. Takahashi, T. Noda, M. Yoshita, H. Sakaki, M. Baba, and H. Akiyama, *Appl. Phys. Lett.* **78**, 3448 (2001).
- <sup>34</sup>F. Bras, P. Boucaud, S. Sauvage, G. Fishman, and J.-M. Gérard, *Appl. Phys. Lett.* **80**, 4620 (2002).